Coherent Dynamics in Complex Elimination Reactions: Experimental and Theoretical Femtochemistry of 1,3-Dibromopropane and Related Systems[†,‡]

Carsten Kötting, Eric W.-G. Diau, Theis I. Sølling, and Ahmed H. Zewail*

Arthur Amos Noyes Laboratory of Chemical Physics, California Institute of Technology, Pasadena, California 91125

Dynamics of the elimination reaction of 1,3-dibromopropane is studied here using femtosecond time-resolved mass spectrometry. It is shown that the complex reaction involving 27 internal degrees of freedom, which is initiated at a total energy of 186 kcal mol^{-1} (corresponding to a n → 5p Rydberg transition), can be described in a reduced space of two coordinates. The first coordinate is the coherent torsional motion involving the two C−Br bonds. The period was observed to be 680 fs. The second coordinate is the C−Br bond-breaking coordinate. The cleavage occurs in 2.5 ps and yields the 3-bromopropyl radical, which subsequently reacts (cleavage of the second C−Br bond and ring closure) to give cyclopropane in 7.5 ps. The reaction channels were identified with the aid of density functional theory calculations. Analyses of orbital populations, energies, and ionization potentials for the different conformations are entirely consistent with the observation of the oscillatory coherent motion and the phase shifts that are observed between certain transients. The interactions of the lone-pairs of the two bromine atoms are shown to be the key for changing the ionization characteristics along the torsional coordinate and thereby enabling the selective probing of vibrational coherence.

I. Introduction

The preparation of a wave packet on excited-state surfaces is the first step in photochemically induced reactions involving the observation of coherent trajectories.[1] The wave packet consists of the superposition of many adjacent vibrational eigenstates and its preparation is unique to the femtosecond (fs) time scale. If the spatial width of the wave packet is sufficiently narrow, the motion is that of a classical particle with well-defined vibrational period(s). The prototype for such behavior is sodium iodide (NaI), where the observed coherent motion describes the resonant trajectories along the reaction coordinate.[2] In polyatomic reactive systems, intramolecular vibrational-energy redistribution (IVR) and the involvement of coordinates perpendicular to the reaction coordinate add to the complexity of the dynamics. However, a reduced nuclear space facilitates a coherent trajectory in such complex systems. One of the first examples of such a behavior was the dissociation reaction of CH_3I,[3,4] where the CH_3-umbrella motion participates additionally to the C−I bond rupture in the reaction dynamics. Other examples include the isomerization of *cis*-stilbene in the gas-phase[5] and, in solution,[6] the multiple step reaction of $(Cr(CO)_6)$,[7] proton transfer in solution,[8] cis−trans isomerization,[9] and processes in biological systems (see, e.g., refs 10−12).

In a recent communication, we reported preliminary studies of coherence in 1,3-dibromopropane (DBP) using femtosecond time-resolved mass spectrometry in a molecular beam.[13] We investigated the wave packet motion on the PES of a n → 5p Rydberg state. The observed modulated signal has a period of 680 fs, which corresponds to the torsional vibration $\delta(CCCBr)$ with a frequency of ∼50 cm^{-1}, as measured by Gustavsen et al. by means of IR spectroscopy.[14] Observation of this motion is possible because of the selectivity in the probing window: Because of the interactions of the lone pair orbitals on the Br atoms, the involved PESs along the torsional coordinate are different; the ground state has a minimum at $\delta(CCCBr) = 60°$, while the cationic ground-state minimum is at 30° and the Rydberg-state minimum is around 45°. Thus, during this vibration the ionization potential (IP) is changing, making the motion detectable by mass spectrometry.

The depopulation of this Rydberg state results from the C−Br bond-breakage, which leads to the intermediate (3-bromopropyl radical) with a time constant of 2.5 ps. Furthermore, the 3-bromopropyl radical intermediate undergoes ring-closure and C−Br bond-cleavage with a time constant of 7.5 ps. Calculations show that other channels are possible but have higher energy barriers. Also, experimental results for labeled 1,3-dibromopropanes show that the decomposition of the 3-bromopropyl radical cannot involve loss or migration of a hydrogen atom. We also studied related systems (Figure 1). The reaction trajectory involves vibrational coherence along the symmetrical $\delta(CCCBr)$ torsion and motion along the C−Br reactive coordinate. This two-dimensional space defines the reactive pathway, which includes not only the bond-rupture coordinate but also the nonreactive mode(s) perpendicular to it, as shown in Figure 2.

In this full account of an early report, we provide details of the experimental results together with those of related halopropanes (Figure 1) and of 2,2-d$_2$-dibromopropane. We also detail

Femtochemistry of 1,3-Dibromopropane

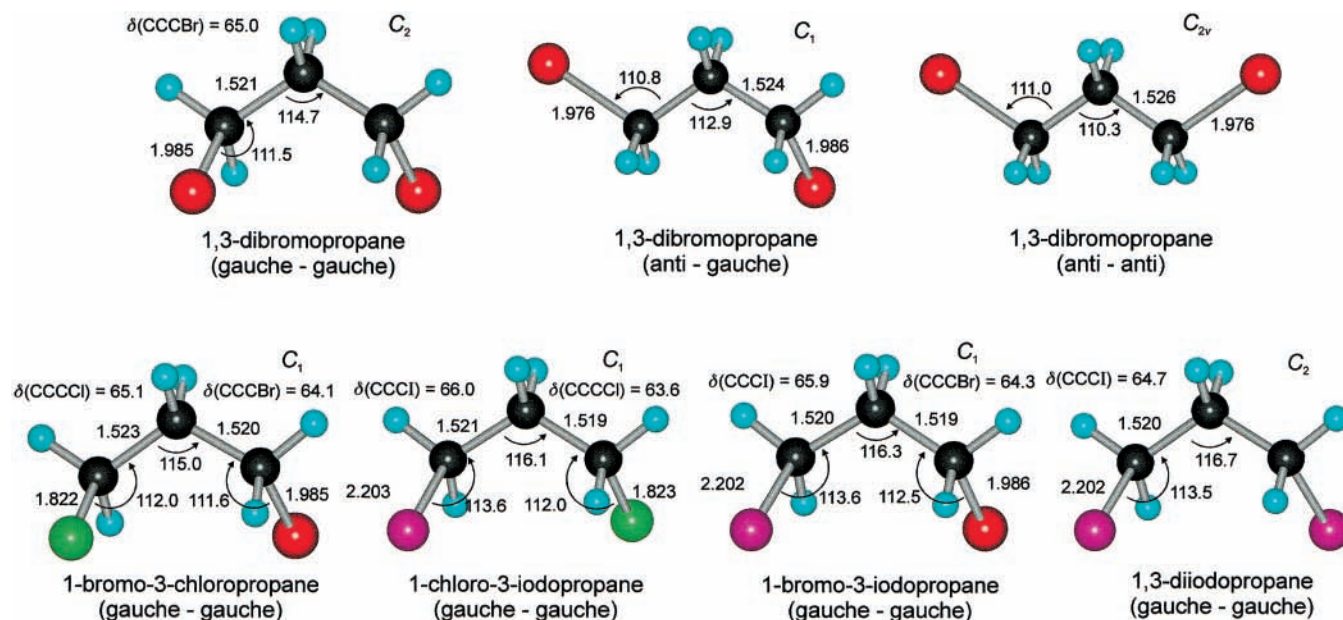*J. Phys. Chem. A, Vol. 106, No. 33, 2002* **7531**

Figure 1. Structures of the three conformers of DBP and of the gauche−gauche conformer of the other investigated dihalocompounds optimized at the B3LYP/6-31G(d,p) (B3LYP/6-311G(d) for the compounds containing iodine) level of theory.

density functional theory (DFT) and time-dependent (TD) DFT calculations for the ground-state, the excited-states, and the cationic ground-state PES's. The excited states of the cation are calculated by means of CASSCF calculations. An extensive analysis of molecular orbitals (MOs) is made here. These results support our reduced two-dimensional model for the dynamics.

II. Experimental and Theoretical Methods

The experimental setup consists of a fs laser system (615 nm, ∼150 μJ pulse^{-1}, ∼80 fs), a molecular beam apparatus and a time-of-flight (TOF) mass spectrometer.[15] The laser system is composed of a colliding-pulse mode-locked (CPM) laser pumped by an Ar$^+$ laser. The output from the CPM is amplified by a four-stage, Nd:YAG-pumped amplifier operating at 20 Hz. The resulting fs pulse was split into two parts to provide the pump and the probe pulse. For the pump, the 615 nm output was frequency doubled, whereas for the probe the 615 nm output was used directly. The time delay was controlled by a translation stage, which alters the path length of the probe pulse. The two beams were spatially combined and focused onto the supersonic molecular beam. Pump and probe beams were appropriately attenuated minimize the background ion signal.
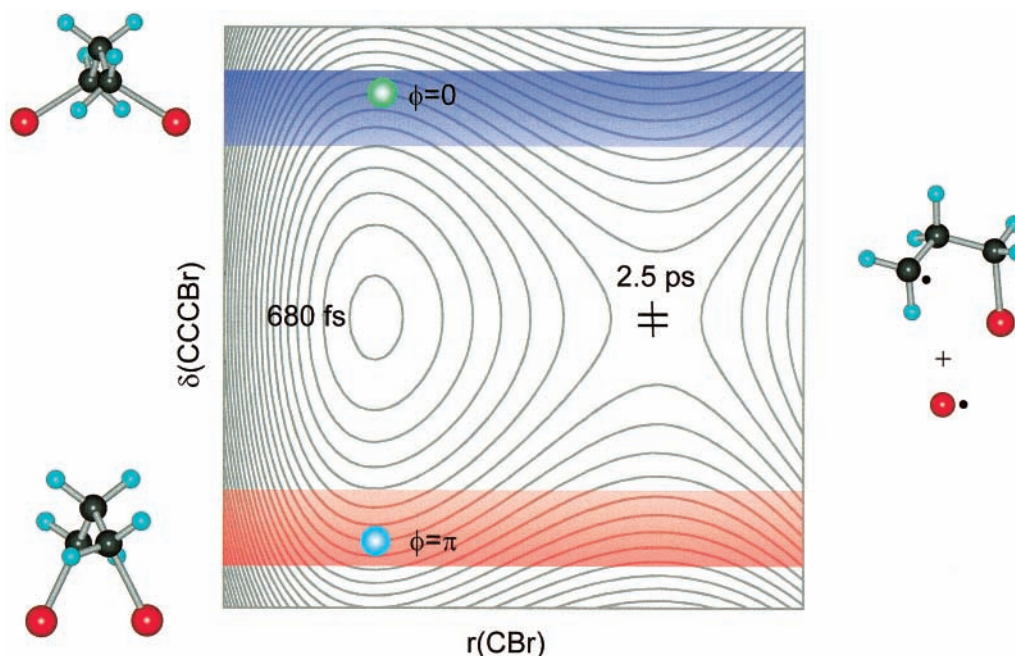

Figure 2. Reduced two-dimensional picture representing the dynamics of the polyatomic system studied here: The nonreactive coordinate corresponds to the torsional vibration, and the reactive coordinate corresponds to the C−Br bond breaking process with a transition state shown as ‡. The two positions shown for the wave packet (green & blue) represent the motion along the nonreactive coordinate for several periods, between the $\delta = 60°$ and $\delta = 30°$ structures, and the subsequent C−Br bond cleavage. Note that the localized fs preparation is essential for the observation of coherence and nonstatistical behavior; the two windows of observation are shown for the phases $\varphi = 0$ (blue) and $\varphi = \pi$ (red). The initial wave packet (not shown) initiates its motion on the repulsive part of the surface.
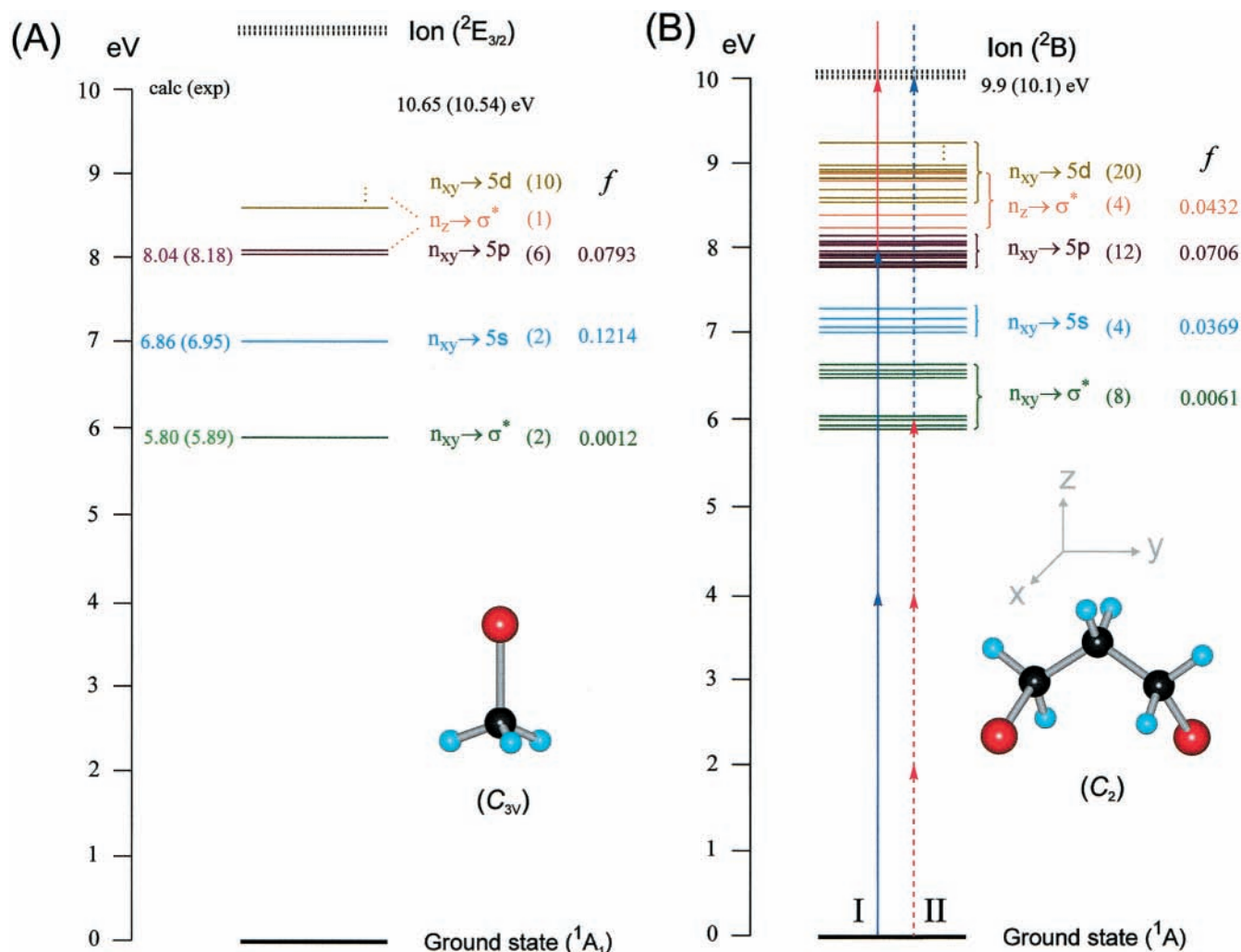
Figure 3. Excitation/ionization scheme for (A) MB and (B) DBP calculated at the TD-B3LYP/6-31+G(d) level of theory. Available experimental values are given in parentheses.[16,23] Spin−orbit coupling is neglected. The types of the transitions are given together with the number of transitions of the same type (in parentheses). The oscillator strengths (*f*) are also calculated values; they refer to one-photon excitations and are therefore only to be used as guidelines.

The polarization angle of the probe beam relative to that of the pump beam was fixed at 54.7° (magic angle). The ions that result from the probe ionization were detected by the (TOF) mass spectrometer.

DBP (99%, Aldrich), 1,3-diiodopropane (99%, Aldrich), 1-bromo-3-chloropropane (99%, Aldrich), 1-chloro-3-iodopropane (99%, Aldrich), and 1-bromopropane (99%, Aldrich) were used without further purification; the mass spectra are consistent with literature spectra.[16] 2,2-d_2-1,3-Dibromopropane and 1-bromo-3-iodopropane were synthesized by procedures described in the literature; refs 17 and 18, respectively. In reported electron diffraction studies, DBP was detected in three different conformations with respect to the rotation along the CC bonds. These are the anti−anti, anti−gauche and the gauche−gauche conformation, as shown in Figure 1. According to these electron diffraction studies, the gauche−gauche conformation is the most stable for DBP, 1,3-diiodopropane, and 1-bromo-3-chloropropane.[19,20] Molecular mechanics calculations indicate that this is also the case for the other investigated 1,3-dihalocompunds.[21]

Calculations were performed using the Gaussian 98 program package.[22] Geometries were calculated using the B3LYP hybrid functional with the 6-31+G(d), 6-31G(d,p), or the 6-311G(d) basis set, as indicated. For all ground-state species, vibrational frequencies were calculated to determine the zero-point energy (ZPE) and the nature of the stationary point in question. Single-

point energies were calculated at the (U) B3LYP/6-311G(d,p) level of theory. In the scans along different coordinates (e.g., r(CBr), δ(CCCBr)), all remaining coordinates were optimized for the ground state at the B3LYP/6-31+G(d) level of theory. The excited-state PESs were obtained by calculating the excitation energies relative to the ground state PESs at the TD-B3LYP/6-31+G(d) level. The energies of the excited states of the cation were calculated at the state-averaged CAS(7,8)/6-31G(d,p) level. The energies of the scans are an upper limit (at the respective level of theory) since relaxation along the other coordinates may lower the energy. To identify the natures of the crossings, a small step size was used.

As a simple model system for which reliable experimental data are available, we used methyl bromide (MB, CH_3Br).[23,24] The calculated vertical excitation energies (TD-DFT) are in excellent agreement with the experimentally determined spectrum (Figure 3A). Note that spin−orbit coupling is neglected in our calculations.

III. Results and Data Analyses

The multiphoton ionization (MPI) mass spectra of DBP and 2,2-d_2-DBP are shown in Figure 4. The peaks corresponding to the parent mass $M^{\bullet+}$ and the fragment mass $[M-Br]^+$ are characterized by a triplet- and a doublet-type pattern. This

Femtochemistry of 1,3-Dibromopropane

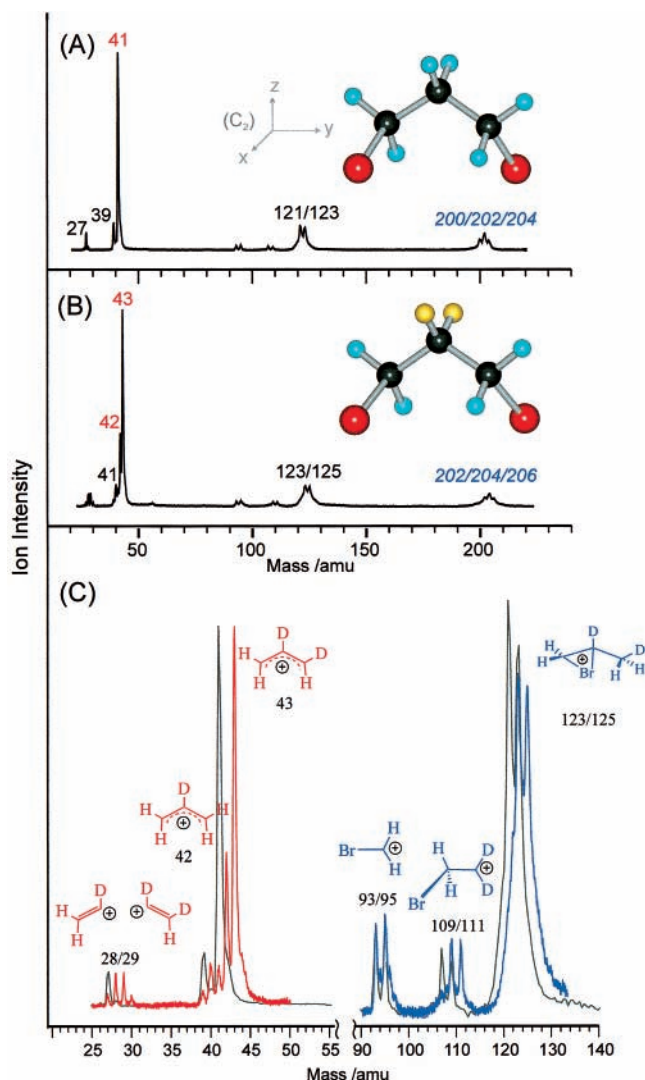*J. Phys. Chem. A, Vol. 106, No. 33, 2002* **7533**

Figure 4. Femtosecond time-resolved mass spectra of (A) DBP and (B) 2,2-d$_2$-DBP obtained at a delay time of ∼50 fs. (C) Enlargement of the most important region in the mass spectra, showing DBP (gray) and 2,2-d$_2$-DBP (red & blue) together with the assignment according to Scheme 1.

appearance is due to the nearly equal abundance of the ^{79}Br and the ^{81}Br isotopes. The base peak is located at 41 amu for DBP. In 2,2-d$_2$-DBP this peak splits into two, a 43 amu (C$_3$H$_3$D$_2$) and a 42 amu (C$_3$H$_4$D). The mechanism for the fragmentation is shown for the 2,2-d$_2$-DBP in Scheme 1: The parent ion (**1**) first cleaves one C−Br bond yielding a primary cation (**2**). The appearance of 121/123 amu (123/125 amu for 2,2-d$_2$-DBP) rather than 120/122 amu proves that the first step in ion fragmentation is indeed the loss of Br and not the loss of HBr/DBr. According to our DFT calculations, this ion shifts a deuterium (hydrogen) in a barrierless reaction leading to the more stable secondary cation (**3**).

The secondary ion is further stabilized by rearrangement into its bridged form (**4**), which corresponds to the global energetic minimum of the C$_3$H$_6$Br$^+$ cation. Alternatively, **4** may also be reached via a four membered heterocyclic ion (**5**). HBr/DBr elimination from **4** will form the allyl cation (**6**), which gives rise to the 41 amu (43/42 amu for 2,2-d$_2$-DBP) signal. The statistical probability for HBr/DBr elimination from **4** is 2:1, consistent with the ∼2:1 ratio of the 43/42 peaks in the mass spectrum of 2,2-d$_2$-DBP. As discussed below, this result is in perfect agreement with the fact that both 42 and 43 amu give the same fs transients. This observation indicates that the ion

signal of 41 amu from DBP (or 42 and 43 amu in 2,2-d$_2$-DBP) actually results from [M−Br]$^+$.[25] The minor signals in the mass spectrum (109/111, 93/95, 27) result from CC bond breakages as shown in Scheme 1.

Figure 5 shows the ion signal as a function of the delay time for the 202, 123, and 41 amu masses of DBP. In Figure 6, the 41 amu transient is shown for delay times up to 30 ps. The transients of the parent 202 amu and the fragment at 123 amu are analogous. Thus, the 123 amu transient signal is mainly due to fragmentation of the parent after ionization. Both transients have three components: (1) a femtosecond response near time zero with time constant τ_0, (2) a coherent modulation of the signal with a period τ_c, combined with an overall decay (and dephasing) with a time constant τ_1, and (3) a negative signal offset. The complementary behavior of the transient for the 41 amu was analyzed similarly: (1) A femtosecond component as in the transient of 202/123 amu, (2) a coherent modulation of the signal with the same period as that of 202/123 amu (τ_c) but with the phase shifted by exactly half a period (π), (3) a buildup and dephasing (time constant τ_1) but with additional decay (time constant τ_2) which is absent in the transient of 202/123 amu, and (4) an offset corresponding to that observed for the 202/123 transients, but now positive. Figure 7 shows the 42 and 43 amu transients for 2,2-d$_2$-DBP. Both transients are identical to the 41 amu transient of DBP.

A relatively strong pump energy is required in order to clearly see the modulation with large S/N. Under such experimental conditions, some DBP is ionized by the pump pulse alone by the absorption of at least three photons (Figure 3B), resulting in a background signal for the parent and fragment masses at negative delay times. The corresponding mass spectrum is shown in Figure 8. At positive delay times, the background ion signal at 202 and 123 amu is constantly decreased, while that at 41 amu is constantly increased, due to parent-ion fragmentation by the probe pulse. This behavior is shown in the mass spectrum (Figure 8) with probe at +3 ps; it explains why a negative signal offset always is obtained in the parent transient (202 amu) and the 123 amu transient and why the offset is positive in the 41 amu transient. Note that the observed femtosecond and picosecond transients nevertheless have to result from a neutral species: An ion fragmenting on the femtosecond or picosecond time scales cannot be detected at the parent mass because the detection in our mass spectrometer takes place on the microsecond time scale.

According to the elementary steps described above, the following consecutive dynamical model for 202, 123, and 41 amu masses is applied to the transients in Figures 4 and 5:

$$A^0 \xrightarrow{\tau_0} A \xrightarrow{\tau_1} B \xrightarrow{\tau_2} C \tag{1}$$

In eq 1, A^0 represents the initial ($t = 0$) Franck−Condon (FC) structure responsible for the fs motion near $t = 0$, A stands for the parent species which undergoes the coherent resonance motion, B stands for the intermediate (3-bromopropyl radical), which only appears in the transient of 41 amu, and C represents the final product, which is dark to our probe. The kinetic equations for each of the species in the above model can be solved (see, e.g., ref 26) to include the instrument response function.[27] The overall transient signal for 202 amu can thus be expressed as $S_{202} = \alpha^0_{202}A^0(t) + \alpha_{202}A(t)$, where $A^0(t)$ is the population of the initial FC species decaying with τ_0 and $A(t)$ is the population of A (buildup by τ_0 and decay by τ_1); α^0_{202} and α_{202} are related to the ionization cross sections and the
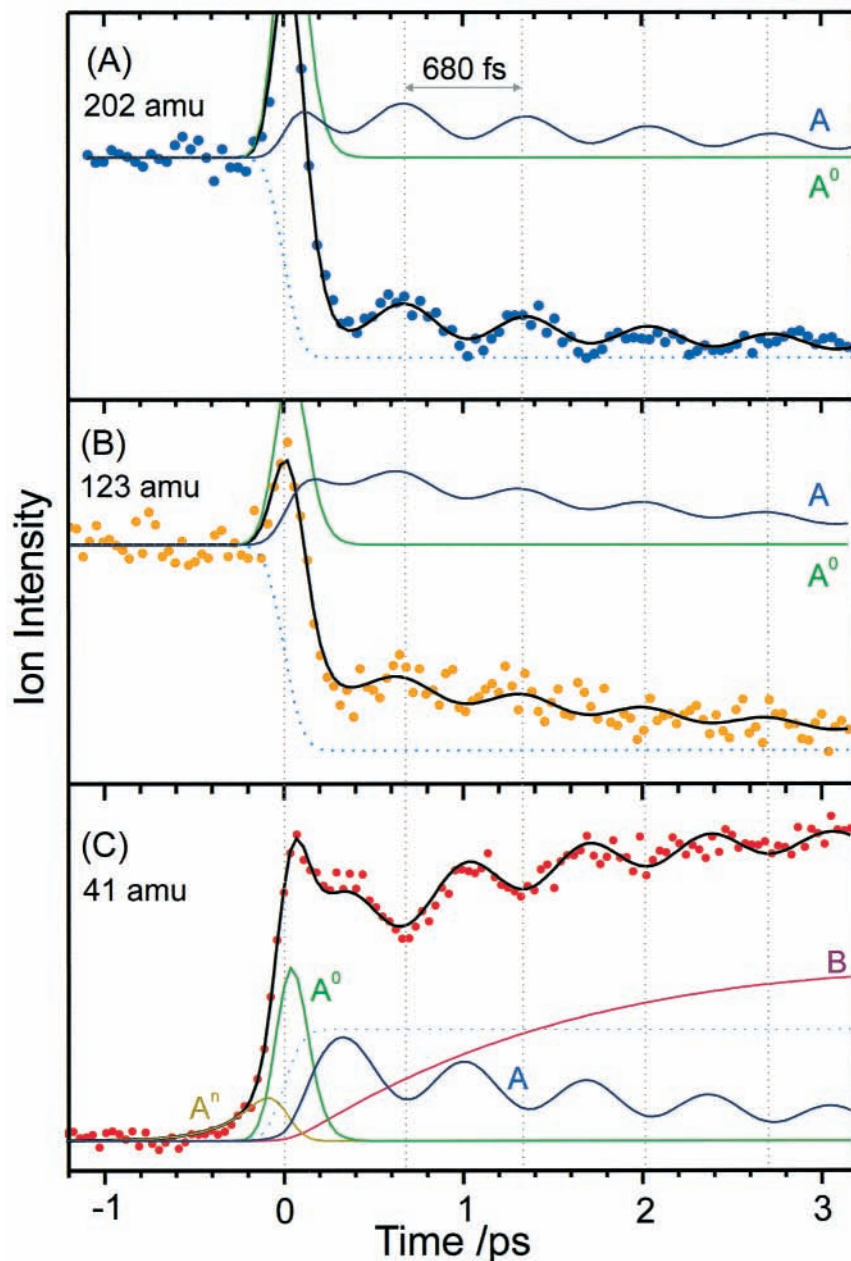
Figure 5. Femtosecond transients of DBP for the parent (202 amu (A)) and the fragment (123 amu(B) and 41 amu (C)) masses, showing the modulated component with a constant period of 680 fs and the phase shift of exactly half a period between the 202/123 and the 41 amu transients. Theoretically obtained curves are also shown, indicating the change of the populations of A^0(green), A (blue), and B (red) according to the kinetic model detailed in the text. The dotted line is the offset described in the model (see text). The small component at negative times, A^n (olive), is due to the process, where the pump/probe scheme is reserved.

efficiency of ion fragmentation. $A(t)$ describes the total population of the species.

The signal must include the probe window detection at a time t to account for the observed coherent motion of the A-molecule trajectories. As shown below, α_{202} depends on the torsional motion δ. The time dependence of this motion can be described by a cosine function with the phase ϕ as shown in Figure 2. Therefore, the signal that reflects the A population must follow

$$S_{202}(A) = \alpha_{202} \{1 + c \cos(t/\tau_c + \phi)\}A(t) \qquad (2)$$

where c is a constant. Note that the average signal over all δ configurations gives only $\alpha_{202}A(t)$ with no coherence. The 123 amu transient can be described by an entirely analogous formula. For the signal of the 41 amu transient, the population of the intermediate $B(t)$ must be additionally included.

Figures 5 and 6 give the comparison between the experimental data and the theoretical curves. Using a nonlinear-least-squares procedure, the best fit of all experimental data gives the following results: $\tau_0 = 50$ fs; $\tau_1 = 2.5$ ps; $\tau_2 = 7.5$ ps; $c = 0.38$. The period obtained is $\tau_c = 680$ fs with the phase $\phi = 0$ (for 202 and 123 amu) and $\phi = \pi$ (for 41 amu). A very good fit was also obtained for the transients of both 42 and 43 amu of 2,2-d_2-DBP using exactly the same time constants and phase shift (Figure 7). This is consistent with the fragmentation of the ion detailed in Scheme 1 because ionization of the transient (3-bromopropyl radical) yields cation **2** which gives rise to the same fragments as the parent ion.

Figure 9 shows the 41 amu transient at different probe pulse intensities. The coherence is most pronounced with a low intensity probe beam. A high probe intensity enhances a small component at negative times. This component can be fitted by

Femtochemistry of 1,3-Dibromopropane

J. Phys. Chem. A, Vol. 106, No. 33, 2002 **7535**

SCHEME 1: Proposed Fragmentation Pathway of the DBP Cation[a]
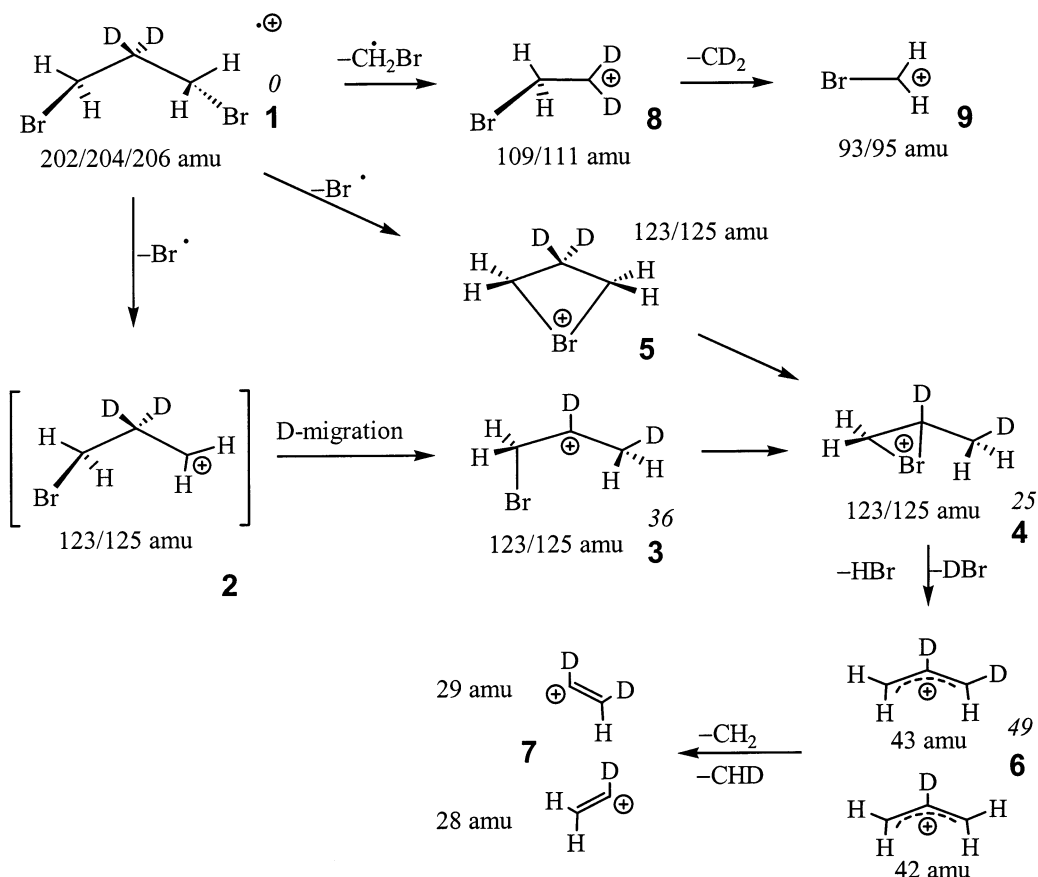
[a] Calculated energies (UB3LYP/6-31G(d,p) + ZPE) are given in italics (kcal mol^{-1}).
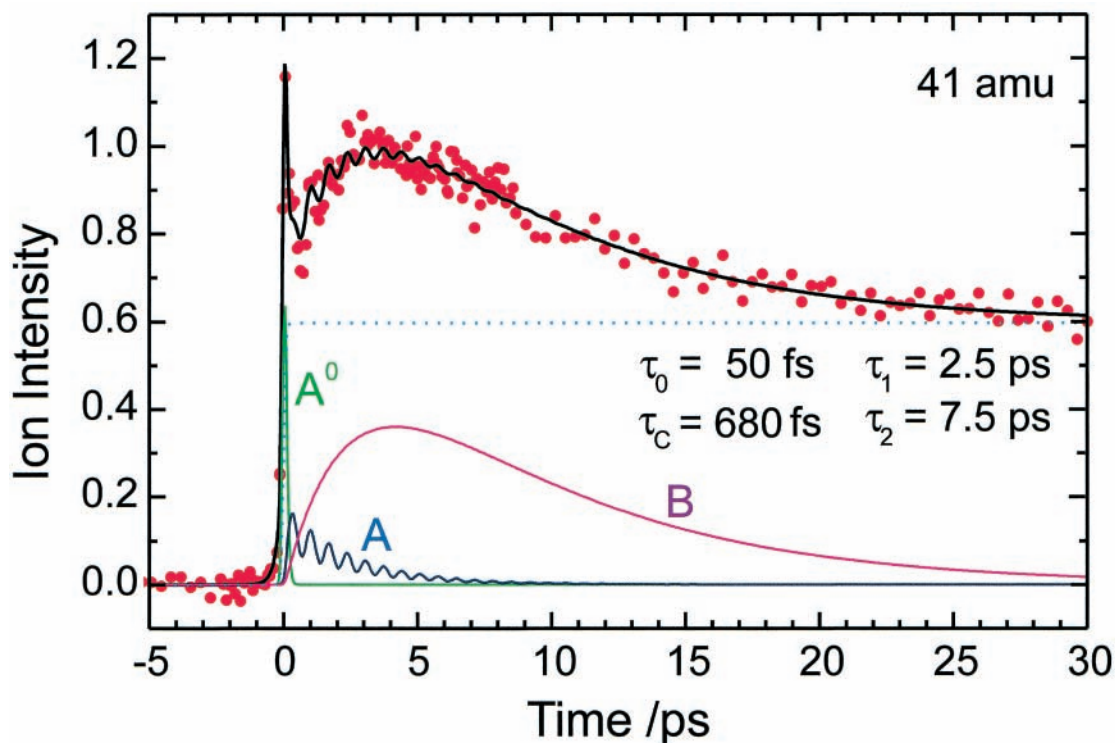

Figure 6. Transient of DBP for the 41 amu species, together with the theoretical fit indicating the signal due to the populations of A^0(green), A (blue), and B (red) according to the kinetic model detailed in the text. The dotted line is the offset described in the model (see text).

a single-exponential function with the decay time constant of 200 fs. This observation is consistent with a simple bond-rupture process that takes place on the $n_{xy} \rightarrow \sigma^*$ repulsive surface along the C−Br bond-breaking coordinate (excitation Scheme II in Figure 3). The intensity of the femtosecond response component strongly increases with larger probe intensity.
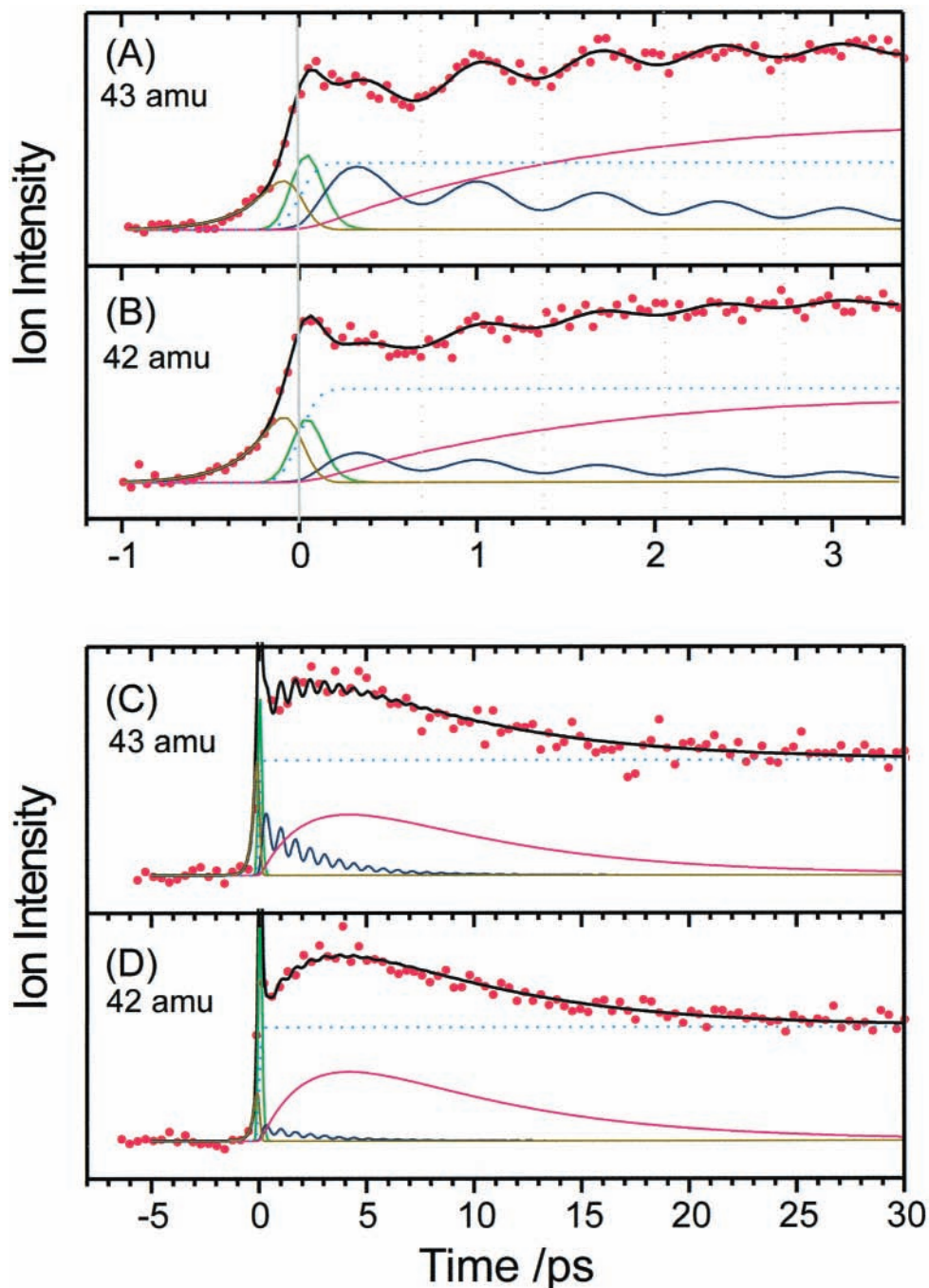
Figure 7. Transients of 2,2-d_2-DBP for the 42 and 43 amu fragment, together with the theoretical fit indicating the signal due to the population of A^0(green), A (blue), and B (red) according to the dynamical model detailed in the text. The dotted line is the offset described in the model (see text).

IV. Discussion

The consecutive model in eq 1 reproduces the observed femtosecond transients for both DBP (Figures 5 and 6) and 2,2-d_2-DBP (Figure 7): The initial femtosecond signal observed in all transients reflects a dephasing process that involves a number of the available degrees of freedom. The initially prepared wave packet moves out of the FC region within the observed 50 fs. After this initial motion, the wave packet executes a coherent vibrational motion with a period of $\tau_c = 680$ fs. The population of this state decays with $\tau_1 = 2.5$ ps, yielding intermediate B, which has a lifetime of 7.5 ps. None of the time constants display changes with deuterium isotopic substitution. In the following, we investigate the electronic structure and reactivity of DBP by means of (TD)-DFT and CASSCF calculations.

A. Molecular Orbitals and the Vertical Excitation Spectrum. To examine the dynamics of DBP in detail, we also investigated a model system—methyl bromide (MB)—for which the experimental gas-phase UV-spectrum is theoretically well established.[23,24] As shown in Figure 3, the excitation spectrum of MB is similar to that of DBP. Figure 10 shows the three highest occupied and the six lowest unoccupied Kohn—Sham (KS) orbitals of MB calculated at the B3LYP/6-31+G(d) level of theory. The occupied orbitals 20—22 correspond to the lone pairs at the bromine atom. The n_z orbital is lower in energy than the two degenerated n_y and n_x orbitals. The LUMO (23) can be described as the σ^* orbital of the C—Br bond. The following energetically higher orbitals (24—28) are Rydberg-type orbitals. The $5p_z$ Rydberg orbital mixes strongly with the $5d_{z^2}$ Rydberg orbital.
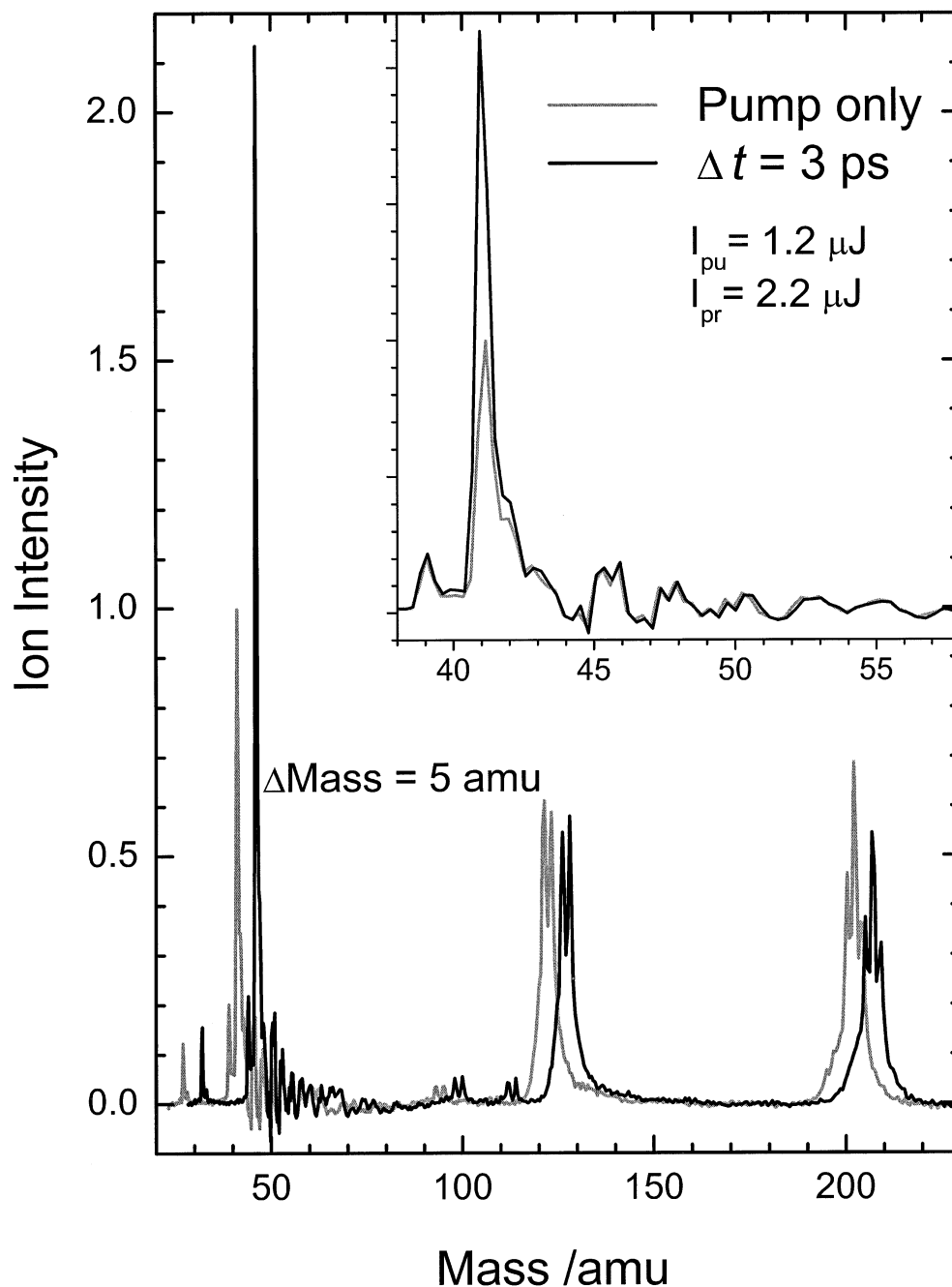
Femtochemistry of 1,3-Dibromopropane

J. Phys. Chem. A, Vol. 106, No. 33, 2002 **7537**

Figure 8. MPI mass spectra of DBP obtained by pump photons only (blue) and pump + probe with a delay time of 3 ps (red). The latter spectrum is shifted by +5 amu for clarity. The pump energy is the same for both spectra.

As illustrated in Figure 3, the 10 lowest singlet excited states are due to excitations of electrons out of the two degenerated n_{xy} orbitals. These are the two $n_{xy} \rightarrow \sigma^*$ states, the two $n_{xy} \rightarrow 5s$ Rydberg and the six $n_{xy} \rightarrow 5p$ Rydberg states. Our calculated excitation energies are shown in Figure 3 together with experimental values derived from the gas-phase UV-spectrum.[23,24] The largest deviation from the experimental value is as low as 0.14 eV. Note that spin−orbit coupling leads to a splitting of all excitations. This splitting is not reproduced because the calculations do not take spin−orbit coupling into account.

The MOs of DBP (Figure 11) are similar to the MOs of MB. Due to the two bromine atoms, there are two n_z, n_x, n_y, and σ^* orbitals, giving rise to eight $n_{xy} \rightarrow \sigma^*$, four $n_{xy} \rightarrow 5s$, 12 $n_{xy} \rightarrow 5p$ and four $n_z \rightarrow \sigma^*$ excitations (for the labeling of the n orbitals,

we use local symmetry, where the C−Br bond describes the z-axes). In agreement with the lower IP of DBP compared with MB (10.1 vs 10.5 eV),[16] the Rydberg states of DBP are slightly lower in energy. Furthermore, because the symmetry is lowered from C_{3v} to C_2, the n_{xy} orbitals are no longer degenerate. The excitation scheme in Figure 3 is as a consequence quite complex. However, the general picture is still the same as in MB. Corresponding excited states are shown with the same color. Our pump pulse promotes DBP, with two 4 eV photons, into a $n_{xy} \rightarrow 5p$ Rydberg state (excitation I in Figure 3).

B. δ(CCCBr) Torsional Coordinate. Note that the polarization shift between the pump and the probe pulses was set at the magic angle (54.7°). The periodic signal persists under these conditions and is therefore due to vibrational coherence.[15,28] The ground-state DBP (C_2 symmetry) has only one vibration with a
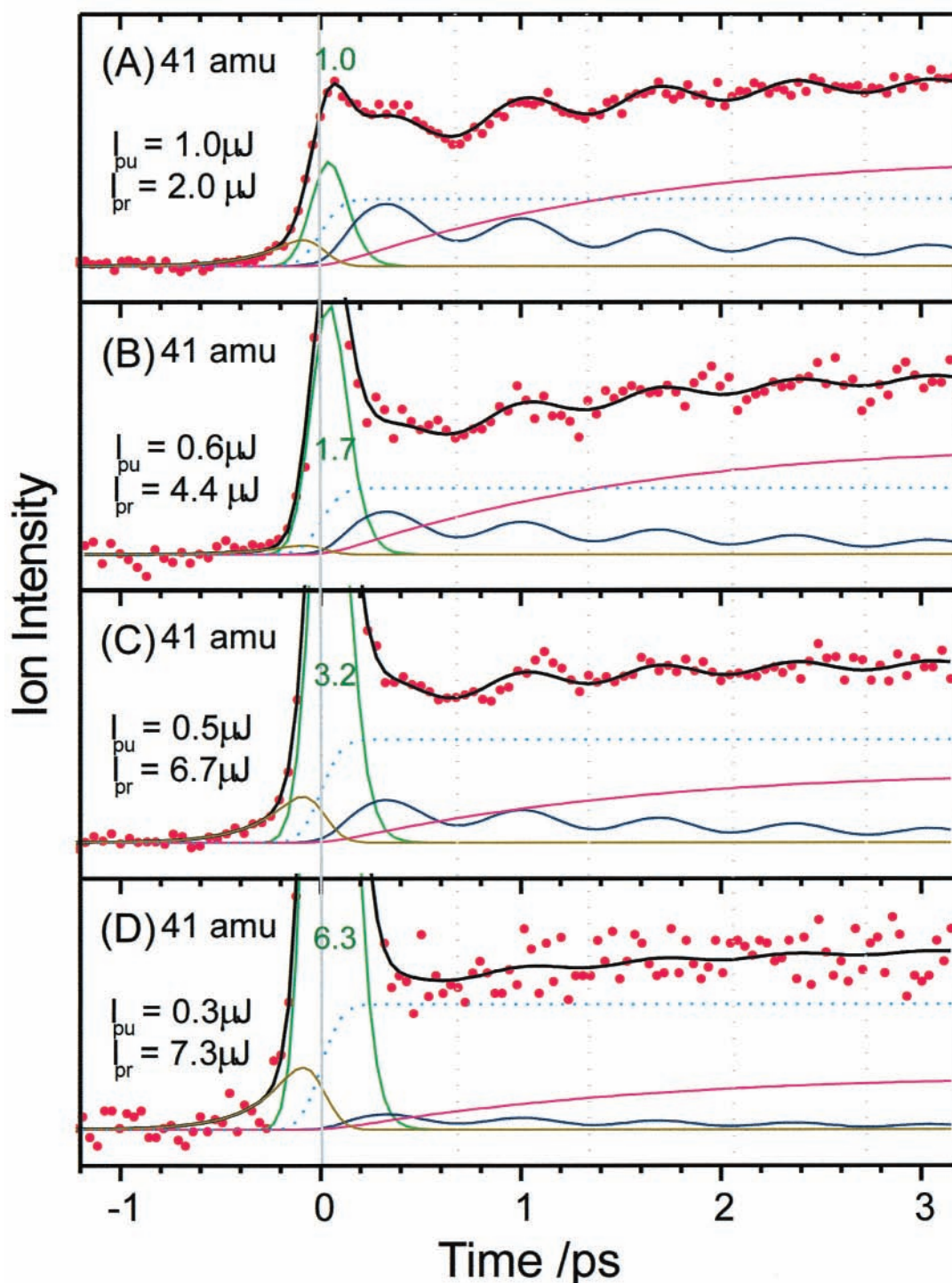
Figure 9. Transients of DBP for the 41 amu fragment, together with the theoretical fit indicating the signal due to the population of A^0(green), A (blue), and B (red) according to the dynamical model detailed in the text. The dotted line is the offset described in the model (see text). The small component at negative times, A^n (olive), is due to a reversed pump/probe scheme.

low frequency ($\sim$50 cm^{-1})[14,19] with a period which is similar to that of the observed coherence ($\tau_c = 680$ fs). This is the δ(CCCBr) torsion with "a" symmetry. According to our TD-DFT calculations of the vertical excitation spectrum of DBP, the absorption of two pump photons brings the molecule into a $n_{xy} \rightarrow 5p$ Rydberg state (Figure 3I). In this particular case, the vibrational modes of the Rydberg excited species can be assumed to be similar to those of the ground state because the bond order does not change during the excitation (it involves a lone-pair electron). Therefore, the observed vibrational coherence can be assigned to the torsional motion that has been

activated upon excitation. In the following, we will give the theoretical foundation of the special features of DBP and its torsional δ(CCCBr) vibration.

The n_{xy} lone pair orbitals of the bromine atoms, which are the four energetically highest occupied MOs (Figure 11, 44–47), are key to the observation of coherence along this coordinate. Due to interactions between the bromine atoms, these orbitals are not degenerate in this case. During the torsional motion the distance between the bromine atoms, and thus their interaction, changes substantially. The interaction is stronger at smaller angles, as shown in Figure 12. The n_y orbitals can
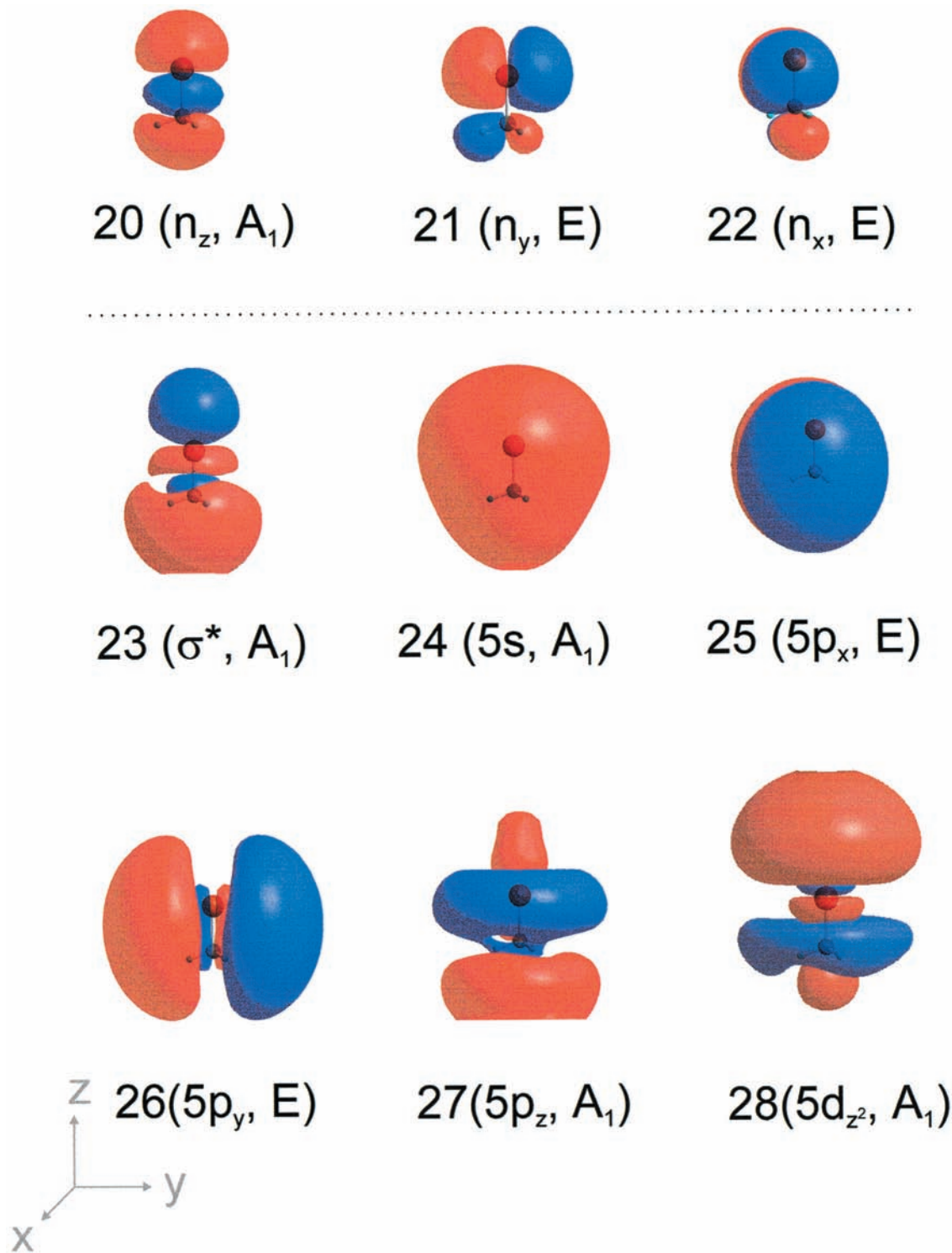
Figure 10. Three highest occupied and the six lowest unoccupied Kohn–Sham orbitals of MB calculated at the B3LYP/6-31+G(d) level of theory.

have either a σ-type bonding or a σ-type antibonding interaction, resulting in a splitting between the two orbitals by more than 1 eV. The n_x orbitals have a similar π-type interaction. In both cases, the energy increase of the antibonding orbitals is larger than the energy decrease of the bonding orbitals. Since all n_{xy} orbitals are doubly occupied in the neutral ground state, the overall energy increases from the minimum ($\delta = 60°$ with a large Br–Br distance of 4.28 Å) along the torsional coordinate toward smaller angles.

On the other hand, in the lowest cationic state, the σ "antibonding" HOMO (n_yB) is only singly occupied. As a result,

the minimum energy of this state is found at $\delta = 30°$ (UB3LYP/6-31+G(d)) with the two Br atoms separated by only 2.89 Å. This is only 0.6 Å longer than in Br_2.[16] The four n_{xy} orbitals provide four low-lying cationic states. In each state, one of these four orbitals is singly occupied. We investigated the behavior of these states along the δ coordinate at the CAS(7,8)/6-31G-(d,p) level of theory, where the active space involves the four n_{xy} orbitals (Figure 12C). At this level, the lowest-energy conformation of the state with the singly occupied n_yB orbital (blue) has $\delta = 35°$. In the case of the state with a singly occupied n_yA orbital (green), this value is $\delta = 65°$; at this angle,
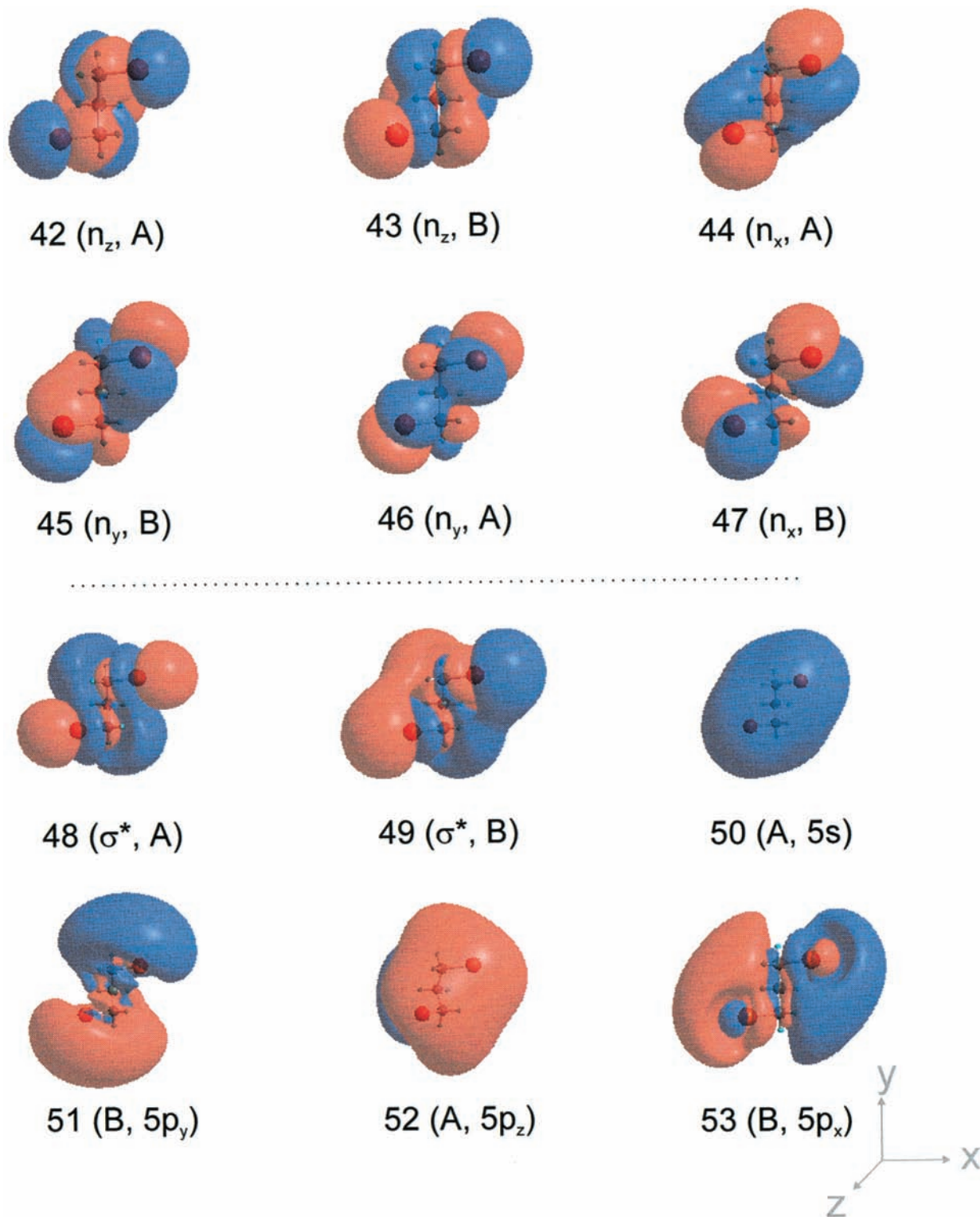
Figure 11. Six highest occupied and the six lowest unoccupied Kohn–Sham orbitals of DBP calculated at the B3LYP/6-31+G(d) level of theory.

this is the lowest-energy state. For the states with singly occupied n_x orbitals (red and orange), the lowest-energy conformation lies in between, at $\delta = 40°$ and $\delta = 50°$, demonstrating the analogous but weaker π-type interaction.

Similarly for the neutral, the 24 excited-state surfaces emerging from excitations of an electron out of the n_{xy} orbitals can be divided into four groups based on the nature of the n_{xy} orbital from which the excitation arises. All states within a group show analogous behavior along the δ coordinate; e.g., all excitations from the n_yB orbital result in a PES similar to the

lowest cationic state. However, due to mixing between the states the picture gets quite complicated. In Figure 13, the four $n_{xy} \rightarrow$ 5s excitations are shown in the same colors as the corresponding ionic states in Figure 12C. The blue PES is due to the $n_yB \rightarrow$ 5s excitation with the minimum at 30° identical to the corresponding cationic state. The PES due to the $n_yA \rightarrow$ 5s excitation (green) has the minimum at an even larger angle than the ground state. Excitations from the n_x orbitals (red and orange) give rise to species for which the lowest-energy conformation lie between these two extrema. Thus, after an
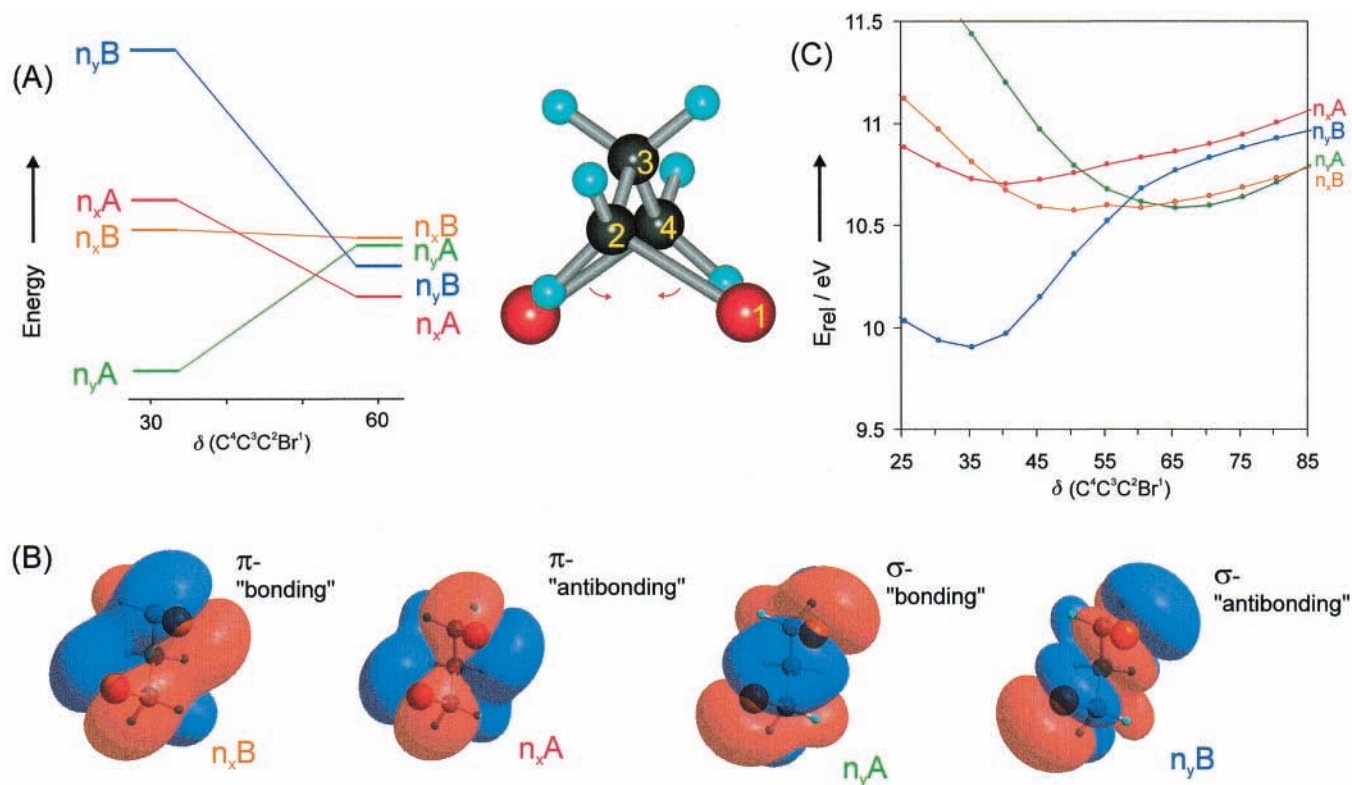
Figure 12. (A) Energy of the four highest occupied molecular orbitals, calculated at the B3LYP/6-31+G(d) level of theory at $\delta = 60°$ (lowest-energy conformation of neutral ground-state DBP) and at $\delta = 30°$ (lowest-energy conformation of cationic ground state). (B) The four highest occupied molecular orbitals at $\delta = 30°$ showing the interaction between the two bromine atoms. (C) The four lowest cationic states calculated at the CAS(7,8)/6-31G(d,p) level along the δ(CCCBr) coordinate.

excitation into these n_x states, the δ motion will be activated by the pump pulse due to the displacement of the PES relative to the ground-state PES, along the δ coordinate (Figure 13). Furthermore, an oscillation around this minimum would lead to an excessive change of the IP, giving rise to different fragmentation after probing (different detection windows) and

allowing for the detection by mass spectrometry. The curve corresponding to the $n_xA \rightarrow 5p_x$ excitation is most likely the one responsible for the observed coherence for two reasons: First, the calculated vertical excitation energy is very close to our excitation energy (8 eV). Second, the torsional frequency can be estimated using a harmonic oscillator model fitted to

SCHEME 2: Candidates for Intermediate B and Their Expected Fragmentation after Ionization
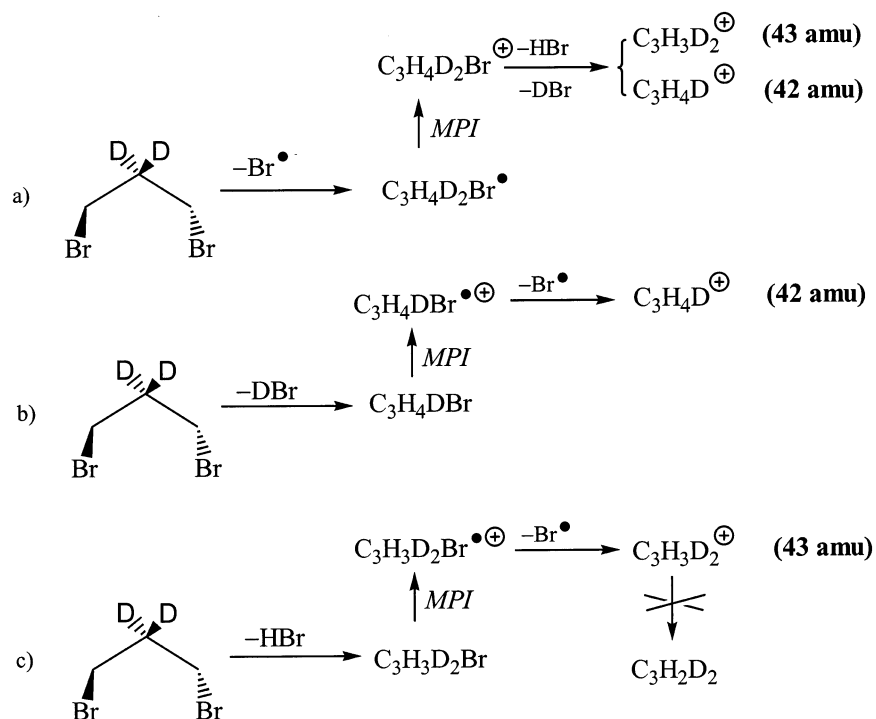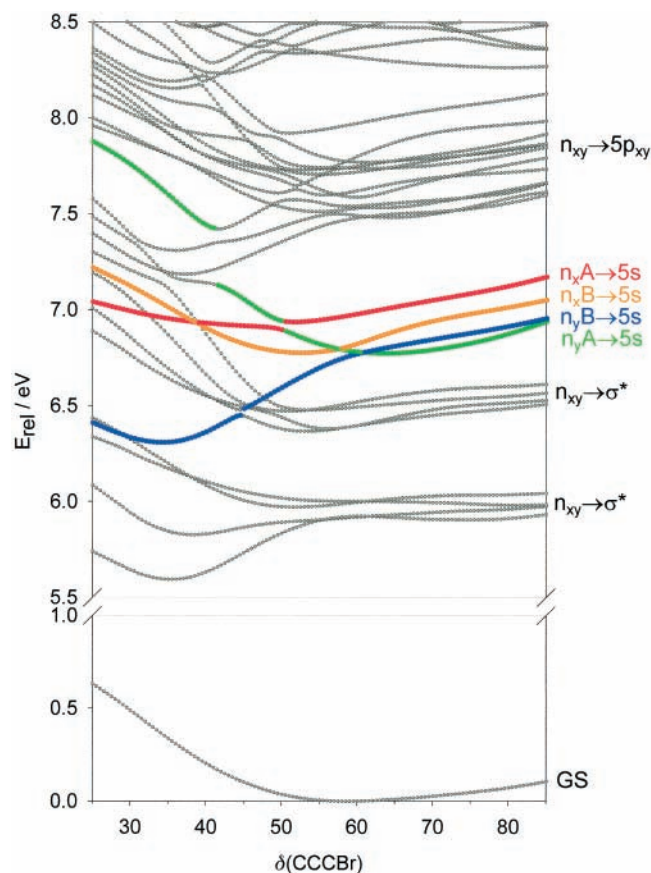
Figure 13. PESs of DBP along the δ(CCCBr) torsional coordinate calculated at the TD-B3LYP/6-31+G(d) level of theory. The four 5s Rydberg surfaces are highlighted ($n_yB \to$ 5s, blue; $n_yA \to$ 5s, green; $n_x \to$ 5s, red and orange). In general, all PES which are due to an excitation of an electron out of the same orbital behave similarly along this coordinate. However, surface crossings and interactions between the surfaces complicate the picture.

Figure 14. Potential energy change along the δ coordinate for the ground state (black), the Rydberg state (red), and the cation (green). The different ionization potentials lead to different content of internal energy in the ionic species, resulting in the most pronounced fragmentation at 30°. This is shown by the longer arrow for the 41 amu species compared to that of the 202 amu species. Since the same overall amount of ions is formed at all conformations, the sum of both signals remains constant. Thus, if the time dependence of the 202 amu species is described by a cosine function, the 41 amu species must be described by the same cosine function with a phase shift of exactly π. Note that the angle in the lower diagram describes the δ(CCCBr) torsional angle, while in the upper diagram it describes the temporal behavior of the cosine. A whole period of the latter is equivalent to the bond torsion from $\delta = 60°$ to $\delta = 30°$ and back to $\delta = 60°$.

the PES of the excited state around the minimum. This calculation gives a value ($\sim$45 cm^{-1}) very close to the one obtained from the observed period of the coherent motion.

The phase shift between the parent and the 41 amu transients is exactly half a period (π). As illustrated in Figure 14, this can be explained by a different amount of fragmentation for the different geometries after ionization for two reasons: First, at a torsional angle of 60°, the density of states is different from that at a torsional angle of 30°. It is reasonable to expect that at 30° more states are available for resonance enhancement, since the ionic states are already accessible by only one probe photon (two pump and one probe photon give a total energy of 10 eV). In turn, more photons will be absorbed at 30°. Accordingly, the ions that are formed from the multiphoton ionization at 30° are, on average, hotter than those formed at 60°. Second, the attractive Br−Br interaction of the 30° species can be maintained during the bond breakage, lowering the transition state for the fragmentation. Both effects lead to less fragmentation after ionization at 60°.

Indeed, the periodical signal of the parent has a maximum at 60° (the initial conformation at $t = 0$) and a minimum at 30° (after half a vibration (π)). Consistently, the fragment signal (41 amu) shows exactly the opposite behavior. From a mathematical point of view, it is apparent that the phase shift must be exactly π: If there is an equal amount of parent molecules that are ionized at all times, then the sum of the parent and fragment signals will be constant, i.e., S(202) + S (41) = const. The time-dependent part of S(202) is cos(t/τ_C), and therefore,
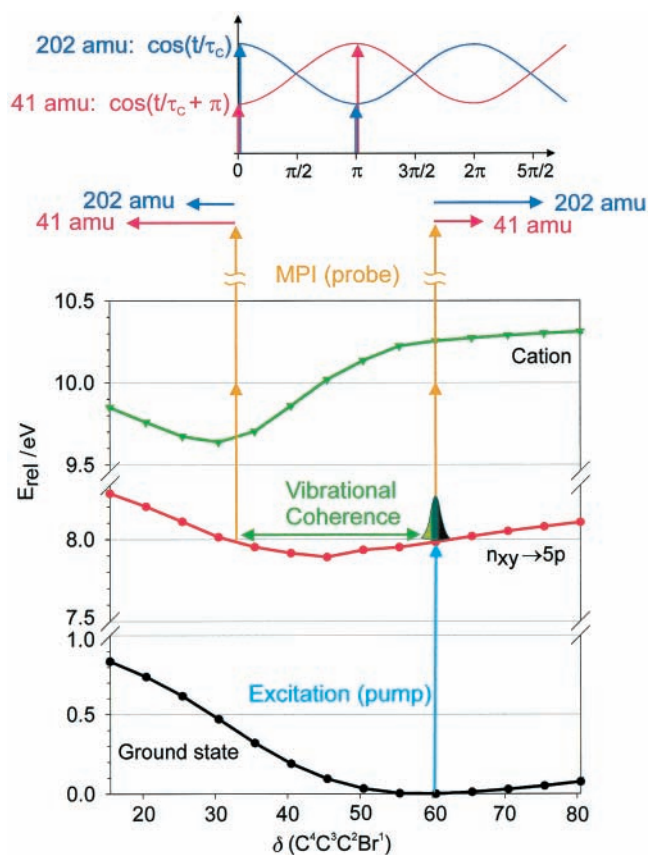
the corresponding part in the 41 amu signal is described by cos(t/τ_C + π).

We also calculated the change of the IP along other normal modes, but in all cases, it is substantially smaller than for the δ motion. Furthermore, a similar δ motion in 1-bromopropane has only a small effect on the IP.

C. Non-Concerted Elimination Dynamics. As described in Section III, the first elementary step occurs with a time constant of $\tau_1 = 2.5$ ps to yield the intermediate B (eq 1). The low-lying σ^* orbitals of the C−Br bond suggest that B is the product of a simple cleavage of this bond, the 3-bromopropyl radical. Since HBr elimination is also energetically possible,[29] we have investigated the dynamics of the reaction of 2,2-d$_2$-DBP. As discussed above (Scheme 1), ionized •CH$_2$CD$_2$CH$_2$Br fragments to both the 42 and 43 amu species (Scheme 2a). Thus, the observation of the same dynamical behavior in both transients indicates their formation from fragmentation of the ionized 3-bromopropyl radical. Accordingly, 3-bromopropyl is intermediate B in eq 1. In contrast, 1,2-DBr elimination would yield allyl bromide (CH$_2$CDCH$_2$Br), to fragment exclusively to the 42 amu species (Scheme 2b), and a 1,3 (or 1,1)-HBr elimination would give only the 43 amu signal (Scheme 2c). Note that the
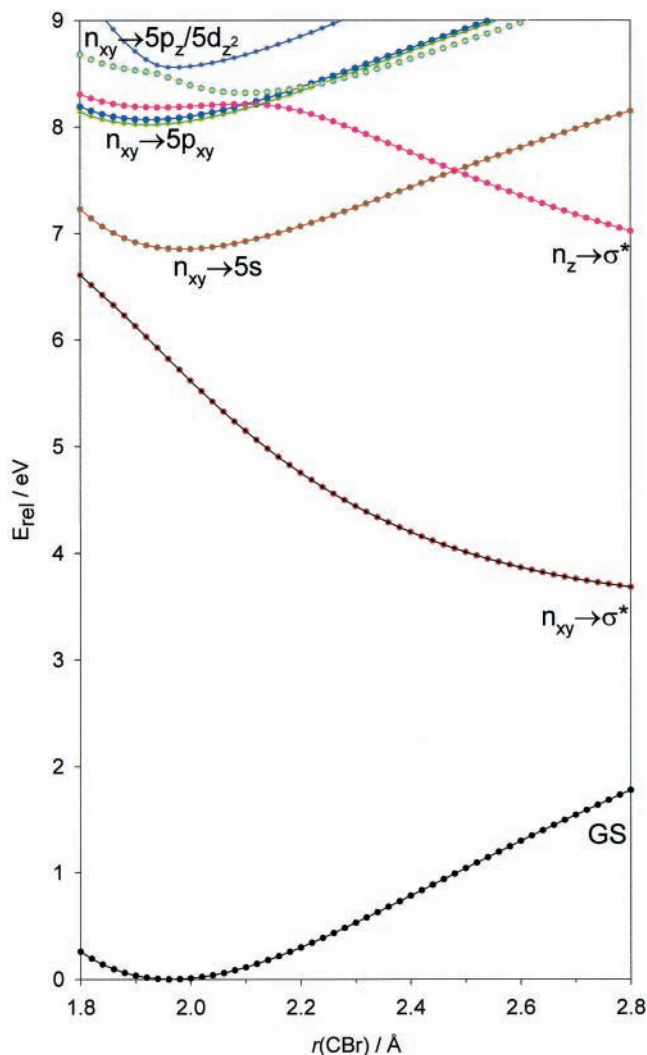
Femtochemistry of 1,3-Dibromopropane

J. Phys. Chem. A, Vol. 106, No. 33, 2002 **7543**

Figure 15. PESs of MB along the r(CBr) bond-breaking coordinate calculated at the TD-B3LYP/6-31+G(d) level of theory.

Figure 16. PESs of DBP along the r(CBr) bond-breaking coordinate calculated at the TD-B3LYP/6-31+G(d) level of theory.

42 amu signal cannot be due to H loss from the 43 amu species because this process is absent for the d_0 compound (no formation of $C_3H_4^{\bullet+}$ (40 amu)). Furthermore, the lack of a kinetic isotope-effect on τ_1 disagrees with the HBr (DBr) elimination mechanism.

The mechanism of the elimination reaction can also be explained by means of MO theory. Figure 15 illustrates the behavior of the singlet excited states along the C−Br bond-breaking coordinate for the model compound MB (under restriction of the C_{3v} symmetry). The two $n_{xy} \rightarrow \sigma^*$ valence states are repulsive, and thus, an excitation to these states would lead to a direct C−Br bond cleavage. The Rydberg states are bounded and resemble the ground state along the r(CBr) coordinate. The next higher repulsive state is the $n_z \rightarrow \sigma^*$ valence state. At the ground-state equilibrium geometry (r(CBr) = 1.98 Å), the $n_z \rightarrow \sigma^*$ state is substantially higher in energy compared to the $n_{xy} \rightarrow 5p$ Rydberg states, but it lies lower than these Rydberg states already at slightly longer C−Br distances. This is not the result of a real surface crossing but of an avoided crossing that arises from mixing of the $n_z \rightarrow \sigma^*$ state with some of the Rydberg states. Accordingly, the diabatic surface—obtained by combining a 5p Rydberg state for small r(CBr) and the $n_z \rightarrow \sigma^*$ state for larger r(CBr)—has a small barrier for the bond breaking process. The analogous surface scan for DBP (Figure 16) shows quite a complex picture, but once again, it is similar to MB. We still find the interaction of the $n_z \rightarrow \sigma^*$ states with
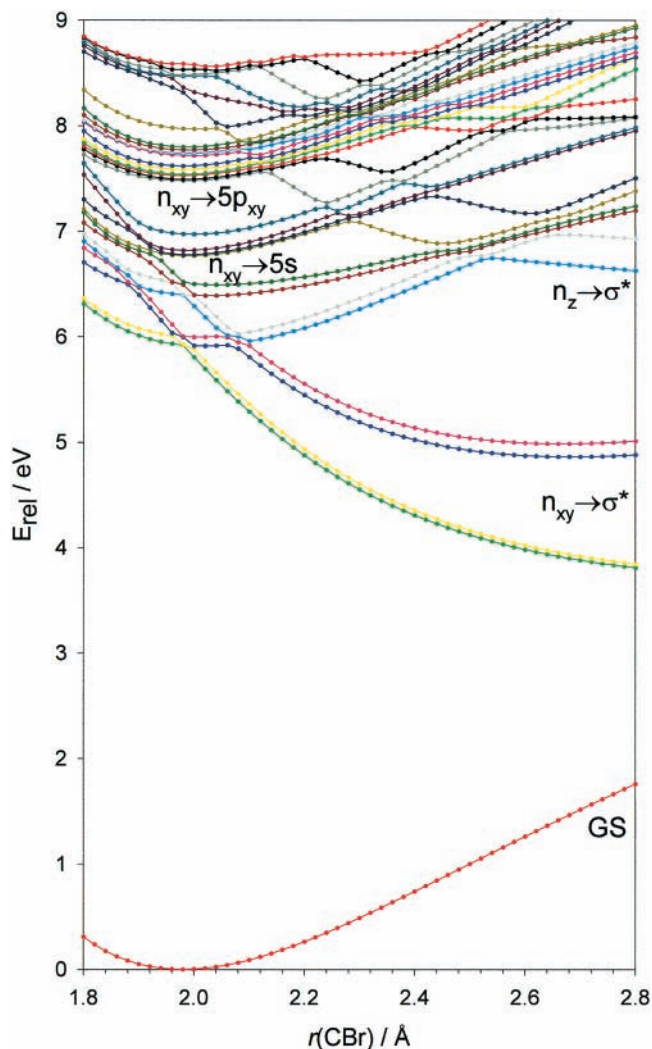
the $n_{xy} \rightarrow 5p$ states, resulting in a diabatic surface with a barrier along the r(CBr) bond breaking coordinate. Note that only half of the $n \rightarrow \sigma^*$ states are repulsive along the r(CBr) coordinate under consideration; the other half are repulsive along the other r'(CBr′) coordinate (not shown). The time constant of 2.5 ps is consistent with the reduced-dimensional picture as shown in Figure 2.

Our calculations also show many curve crossings between the $n_xA \rightarrow 5p_x$ Rydberg state and the other (n,5p) Rydberg states along the δ coordinate (Figure 13). Therefore, it is also possible for the C−Br bond-breaking process to occur through the lower repulsive $n_{xy} \rightarrow \sigma^*$ surfaces, which may be reached by Landau− Zener crossings of excited-state surfaces. On one hand, such a cascading down along the δ coordinate could also be detected since this motion is sensitive to our probe. However, one would expect a more complicated pattern and not a simple cosine form, since the surfaces have different slopes and cross at different angles. Furthermore, the data can be fitted with $\phi = 0$, so it is more likely that coherence is due to movement of the wave packet on the initially excited state. All our experimental and theoretical evidence supports the fact that the observed transients reflect the C−Br bond-breaking process, which yields the 3-bromopropyl radical as the intermediate B in eq 1.

D. Chemistry of the 3-Bromopropyl Radical. Figure 17 illustrates the possible reaction pathways for the 3-bromopropyl radical. The lowest barrier (17 kcal mol^{-1} at the B3LYP/
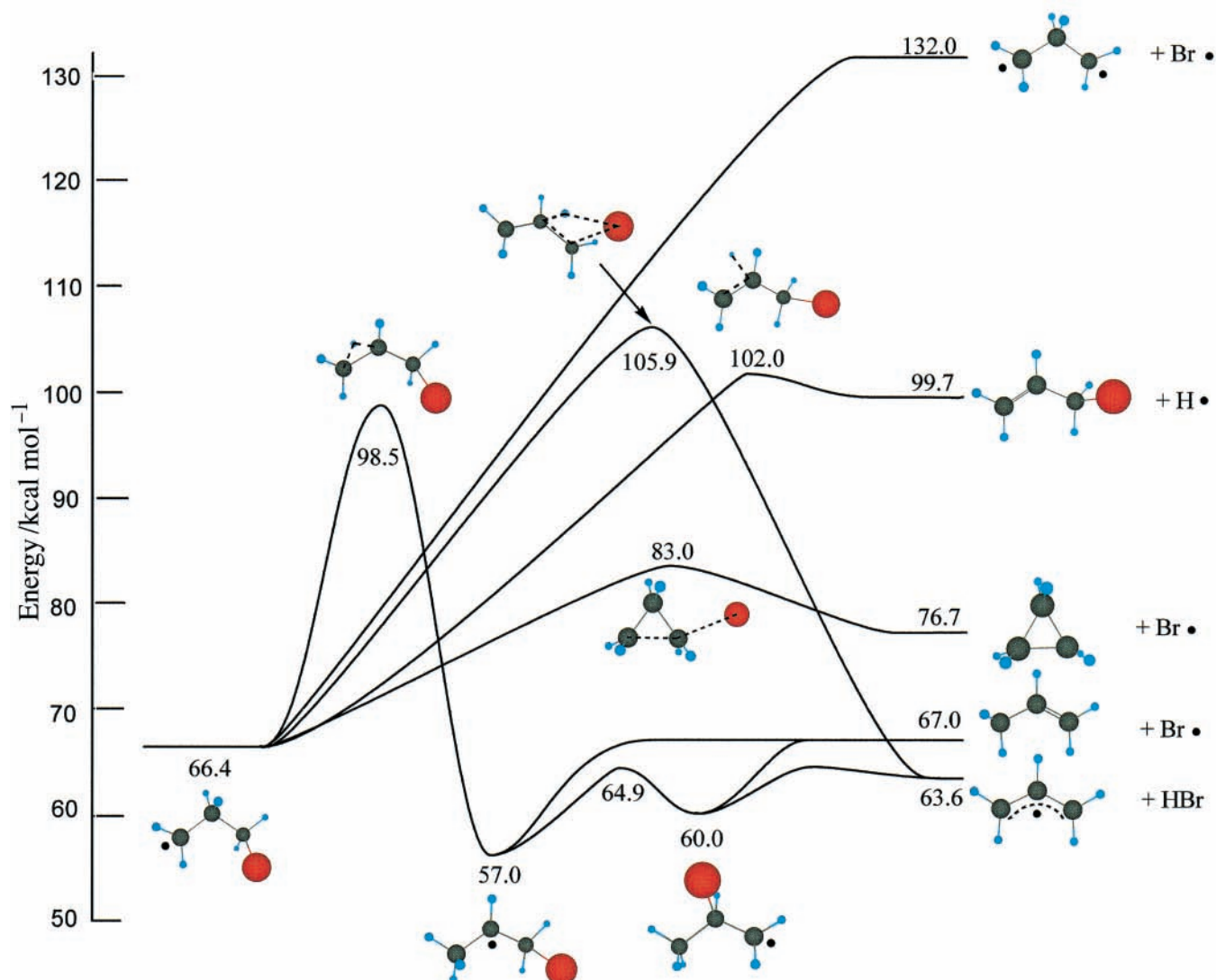
Figure 17. Reaction coordinate diagram of the global ground-state PES of C_3H_6Br along different reaction channels. The stationary points are calculated at the B3LYP/6-311G(d,p)//B3LYP/6-31G(d) level of theory with ZPE corrections.

6-311G(d,p)//B3LYP/6-31G(d,p) + ZPE level of theory) was calculated for the concerted Br elimination/ring-closure reaction to yield cyclopropane and a bromine atom as the final products. The transition state is consistent with that calculated for the bromination of cyclopropane.[30] However, since the ring closure is entropically disfavored, other reactions cannot be ruled out completely. Possible competing reactions are the elimination of a hydrogen atom in the 2-position yielding 3-bromopropene with a 36 kcal mol^{-1} barrier and the elimination of HBr yielding the allyl radical with a 40 kcal mol^{-1} barrier or a 1,2-H shift yielding 1-bromoprop-2-yl radical with a 32 kcal mol^{-1} barrier. The latter product can shift the bromine atom very easily leading to the 2-bromopropyl radical, which can eliminate the bromine atom to give propene or HBr to give the allyl radical. The HBr eliminations are highly asynchronous. In the transition state, the C–Br bond is already lengthened substantially, but the C–H bond is not. Consequently, the transition state for the elimination from the 3-bromopropyl radical resembles a 1,3 diradical, but the transition state for the elimination from the 2-bromopropyl radical resembles an alkene, and it is thus lower in energy by about 41 kcal mol^{-1}. Simple cleavage of the second C–Br bond without concerted ring closure (forming trimethylene) has an energy demand that is higher by 49 kcal mol^{-1} and can therefore be disregarded.

In our experiments, we observe a lifetime of 7.5 ps for both DBP and 2,2-d$_2$-DBP. The combined bromine elimination/ring closure process is the only reaction that does not involve a deuterium in the 2,2-d$_2$-DBP. Thus, both the experimental absence of an isotope effect and the computational result of the lowest barrier for this process are consistent with the formation of cyclopropane as the principal product.

E. Early Time Behavior. A femtosecond component at $t = 0$ is common in our experiments and can result from three different effects. The first is the dephasing of the wave packet out of the FC region. At $t = 0$, the internal kinetic energy is very low because in the molecular beam the temperature of the molecules is close to zero. After the excitation, the wave packet moves downhill on the PES. This involves several coordinates and therefore different time constants. The recurrence of the initial wave packet is only possible within a reasonably short time if these time constants are commensurate. The second effect is related to resonance-enhanced multiphoton ionization, when both pump and probe pulses are present. Under this condition, more combinations of pump/probe energies are possible, and thus, more resonance states are accessible. In the case of DBP, there is a resonant state at 6 eV, which can be reached by either three probe or by one pump and one probe photons. Once this state is accessed, absorption of additional photons is relatively
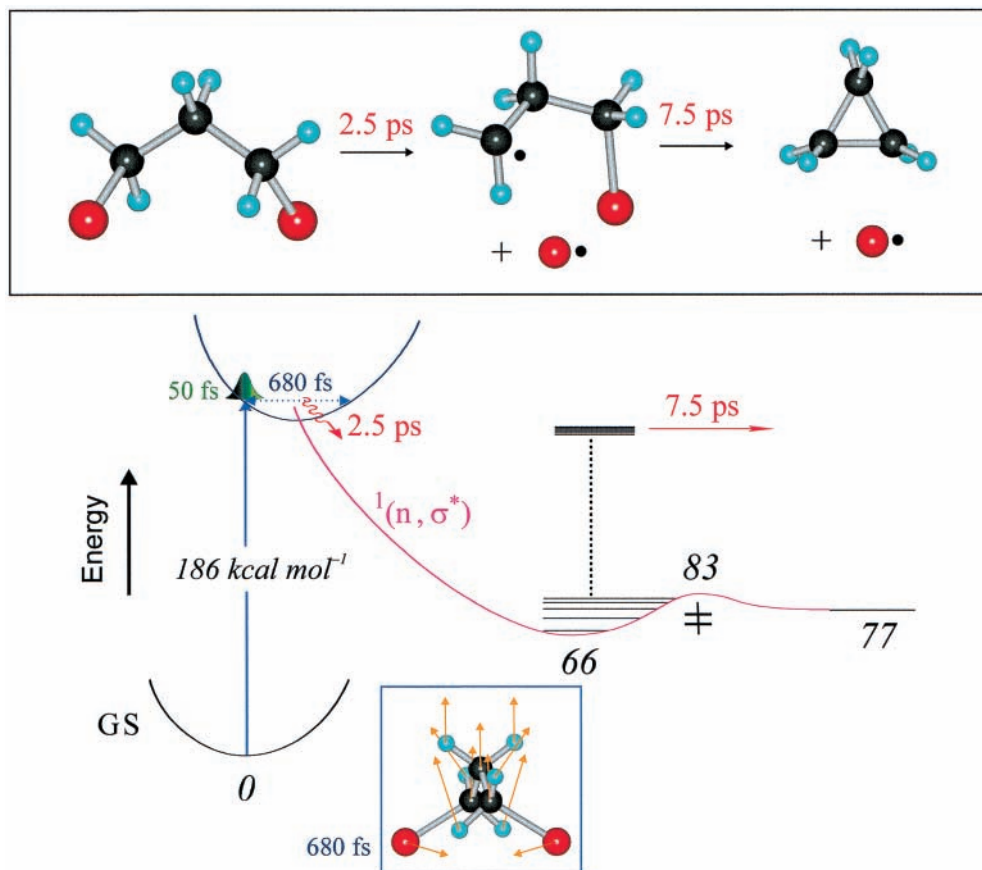
Femtochemistry of 1,3-Dibromopropane

J. Phys. Chem. A, Vol. 106, No. 33, 2002 **7545**

Figure 18. Molecular structures and reaction coordinate (RC): Shown are the time scales involved and the values for the energies (relative to the ground state) in kcal mol^{-1}, calculated at the B3LYP/6-311G(d,p)//6-31G(d,p) level of theory with ZPE corrections. The inset shows the calculated normal-coordinate vectors for the ground-state torsional vibration.

easy since the electronic states are close and it is likely that the system will reach another resonant state. Finally, the effect could be due to a bifurcation of the wave packet resulting in a fraction of the molecules reacting at a different time scale. However, if this would be the case we expect a corresponding rise in the product signal (41 amu). The absence of this rise in the 41 amu signal suggest that the early time behavior is due to the first two effects.

F. Excitation to the $n_{xy} \rightarrow \sigma^*$ State. In the transients, we observed a component with a low signal intensity at negative times (Figure 5C). Its behavior in time can be described by a single-exponential decay with a time constant of 200 fs. At negative times, the sequence of pump and probe is reversed. As shown in Figure 3(II), we can pump DBP with three 2 eV photons to reach a $n_{xy} \rightarrow \sigma^*$ state. The ionization process is then induced by the 4 eV photons. From the results in Figure 16, one notices that the $n_{xy} \rightarrow \sigma^*$ states are repulsive along the C−Br coordinate, in line with the observed ultrafast decomposition. In this case, the bond cleavage does not involve a second coordinate.

G. Other Halocompounds. We have also investigated $BrCH_2CH_2CH_3$ and the 1,3-dihalopropanes $BrCH_2CH_2CH_2Cl$, $BrCH_2CH_2CH_2I$, $ClCH_2CH_2CH_2I$, and $ICH_2CH_2CH_2I$ with the same experimental setup and photon energies. The gauche−gauche conformation is the most stable for all investigated dihalopropanes.[20,21,31] The calculated geometries (Figure 1) obtained from our DFT calculations are very similar to each other, and all compounds have the symmetrical torsional motion δ(CCCX) as the normal mode with the lowest frequency (Table 1 and Figure 18). However, none of them showed any vibrationalcoherence. In all cases, the initial excited state has a

TABLE 1: Time Constants Related to the Reactions and the Torsional Motion of the Investigated Compounds[a]

	τ_0	τ_1	τ_2	$\tau_{\nu(CCCX),exp}$	$\tau_{\nu(CCCX),calc}$[b]
DBP	50	2500	7500	680	670
2,2-d$_2$-DBP	50	2500	7500	680	670
H(CH$_2$)$_3$Br		80	5500		230
Cl(CH$_2$)$_3$Br		270	7000		560
I(CH$_2$)$_3$Cl		<100			640
I(CH$_2$)$_3$Br		<100			790
I(CH$_2$)$_3$I		<100			880

[a] Values in fs. [b] Calculated at the B3LYP/6-31G(d,p) (B3LYP/6-311G(d,p) for the compounds containing iodine) level of theory for the ground-state species.

lifetime shorter than the expected period of the torsional vibration. The time constants are shown in Table 1.

All compounds containing iodine react after absorbing only one 4 eV photon because the σ^* orbital of the C−I bond is lower than the σ^* orbital of the C−Br bond.[32] According to our calculations, this state is repulsive and the C−I bond cleaves on the femtosecond time scale, which is exactly what we observe. This is similar to the properties of the probe photon excitation of DBP described in section IV.F. The transients can be fitted as a single-exponential decay with $\tau_1 < 100$ fs.

In 1-bromo-3-chloropropane, we observed the two-photon excitation. The transients were treated theoretically (eq 1) as for DBP but without the involvement of τ_0. The intermediate radical, again observed at 41 amu, is formed with a time constant of $\tau_1 = 270$ fs. This is faster than the expected period of a coherent motion ($\tau_c = 560$ fs), which consequently could not be observed. In 1-bromopropane, A decays by $\tau_1 = 80$ fs. The intermediate B decays within $\tau_2 = 7$ ps for 1-bromo-3-

chloropropane and 5.5 ps for 1-bromopropane. Excitations with different energies might promote the molecules to sufficiently long-lived Rydberg states with similar properties as the one observed for DBP, since an analogous behavior of the Rydberg states and the cationic states along the δ coordinate is expected.

It is important to note that in 1-bromopropane there is no resonance interaction between two bromine atoms, hence the decrease in selectivity of probing coherence. However, as mentioned above, the time scale for the decay of 1-bromopropane is faster, and resonances are therefore not observed.

V. Conclusion

Excitation of DBP into a 5p-Rydberg state leads to the cleavage of a C—Br bond with a time constant $\tau_1 = 2.5$ ps. The intermediate 3-bromopropyl radical has a lifetime of 7.5 ps. It decomposes to form cyclopropane as the energetically favored product (Figure 17). The dynamics of the first bond breakage was observed, not only along the C—Br bond-breaking coordinate, but also along the δ(CCCBr) torsional coordinate. This is because the change of the IP along this coordinate provides selectivity in the detection window along the torsional coordinate when MPI mass spectrometry is utilized.

These results demonstrate the reduced dimensionality (2 out of 27 degrees of freedom) and persistence of coherence in this elimination reaction. All findings are supported by the results of DFT and TD-DFT calculations. The experimental observation of coherent trajectories in polyatomic systems is the consequence of femtosecond coherent preparation and will be suppressed (mimicking a statistical behavior) if microcanonical-state preparation is involved.[33,34]

References and Notes

(1) Zewail, A. H. *J. Phys. Chem. A* **2000**, *104*, 5660−5694, and references therein.

(2) Mokhtari, A.; Cong, P.; Herek, J. L.; Zewail, A. H. *Nature* **1990**, *348*, 225−227.

(3) Janssen, M. H. M.; Dantus, M.; Guo, H.; Zewail, A. H. *Chem. Phys. Lett.* **1993**, *214*, 281−289.

(4) Guo, H.; Zewail, A. H. *Can. J. Chem.* **1994**, *72*, 947−957.

(5) Pedersen, S.; Bañares, L.; Zewail, A. H. *J. Chem. Phys.* **1992**, *97*, 8801−8804.

(6) Szarka, A. Z.; Pugliano, N.; Palit, D. K.; Hochstrasser, R. M. *Chem. Phys. Lett.* **1995**, *240*, 25−30.

(7) Trushin, S. A.; Fuss, W.; Schmid, W. E.; Kompa, K. L. *J. Phys. Chem. A* **1998**, *102*, 4129−4137.

(8) Lochbrunner, S.; Wurzer, A. J.; Riedle, E. *J. Chem. Phys.* **2000**, *112*, 10699−10702.

(9) Takeuchi, S.; Tahara, T. *Chem. Phys. Lett.* **2000**, *326*, 430−438.

(10) Sundström, V. *Femtochemistry and Femtobiology: Ultrafast Reaction Dynamics at Atomic-Scale Resolution*; Imperial College Press: World Scientific Publishing: Singapore, 1996.

(11) Gonzalez-Luque, R.; Garavelli, M.; Bernardi, F.; Merchan, M.; Robb, M. A.; Olivucci, M. *Proc. Natl. Acad. Sci. U.S.A.* **2000**, *97*, 9379−9384.

(12) Eaton, W. A. *Proc. Natl. Acad. Sci. U.S.A.* **1999**, *96*, 5897−5899.

(13) Kötting, C.; Diau, E. W.-G.; Baldwin, J. E.; Zewail, A. H. *J. Phys. Chem. A* **2001**, *105*, 1677−1682.

(14) Gustavsen, J. E.; Klaeboe, P.; Stølevik, R. *J. Mol. Struct.* **1978**, *50*, 285−291.

(15) Zewail, A. H. *Femtochemistry: Ultrafast Dynamics of the Chemical Bond*; World Scientific: Singapore, 1994; Vols. I and II.

(16) Mallard, W. G.; Linstrom, P. J., Eds.; *NIST Chemistry WebBook, NIST Standard Reference Database Number 69*; National Institute of Standards and Technology: Gaithersburg, MD, 2000.

(17) Baldwin, J. E.; Patel, D. B. *J. Labeled Compd. Radiopharm.* **1999**, *42*, 55−61.

(18) House, H. O.; Sayer, T. S. B.; Yau, C.-C. *J. Org. Chem.* **1978**, *43*, 2153-2157.

(19) Farup, P. E.; Stølevik, R. *Acta Chem. Scand. A* **1974**, *28*, 680−692.

(20) Postmyr, L. *J. Mol. Struct.* **1994**, *319*, 211−221.

(21) Postmyr, L. *J. Mol. Struct.* **1993**, *298*, 137−145.

(22) Frisch, M. J.; Trucks, G. W.; Schlegel, H. B.; Scuseria, G. E.; Robb, M. A.; Cheeseman, J. R.; Zakrzewski, V. G.; Montgomery, J. A.; Stratmann, R. E.; Burant, J. C.; Dapprich, S.; Millam, J. M.; Daniels, A. D.; Kudin, K. N.; Strain, M. C.; Farkas, O.; Tomasi, J.; Barone, V.; Cossi, M.; Cammi, R.; Mennucci, B.; Pomelli, C.; Adamo, C.; Clifford, S.; Ochterski, J.; Petersson, G. A.; Ayala, P. Y.; Cui, Q.; Morokuma, K.; Malick, D. K.; Rabuck, A. D.; Raghavachari, K.; Foresman, J. B.; Cioslowski, J.; Ortiz, J. V.; Stefanov, B. B.; Liu, G.; Liashenko, A.; Piskorz, P.; Komaromi, I.; Gomperts, R.; Martin, R. L.; Fox, D. J.; Keith, T.; Al-Laham, M. A.; Peng, C. Y.; Nanayakkara, A.; Gonzalez, C.; Challacombe, M.; Gill, P. M. W.; Johnson, B. G.; Chen, W.; Wong, M. W.; Andres, J. L.; Head-Gordon, M.; Replogle, E. S.; Pople, J. A. *Gaussian98*, Revision A.9; Gaussian, Inc.: Pittsburgh, PA, 1998.

(23) Causley, G. C.; Russell, B. R. *J. Chem. Phys.* **1975**, *62*, 848−857.

(24) Felps, W. S.; Rupnik, K.; McGlynn, S. P. *J. Phys. Chem.* **1991**, *95*, 639−656.

(25) Danon, A.; Amirav, A. *J. Phys. Chem.* **1989**, *93*, 5549−5562.

(26) Steinfeld, J. I.; Francisco, J. S.; Hase, W. L. *Chemical Kinetics And Dynamics*, 2nd ed.; Prentice Hall: Upper Saddle River, NJ, 1999.

(27) Pedersen, S.; Zewail, A. H. *Mol. Phys.* **1996**, *89*, 1455−1502.

(28) Baskin, J. S.; Zewail, A. H. *J. Phys. Chem. A* **2001**, *105*, 3680−3692.

(29) Benson, S. W.; Bose, A. N. *J. Chem. Phys.* **1963**, *39*, 3463−3473.

(30) Coxon, J. M.; Smith, W. B. *J. Org. Chem.* **2000**, *65*, 2192−2194.

(31) Aksnes, D. W. *Magn. Reson. Chem.* **1989**, *27*, 246−248.

(32) Penner, A.; Amirav, A. *J. Chem. Phys.* **1990**, *93*, 8576−8579.

(33) Diau, E. W.-G.; Herek, J.; Kim, Z. H.; Zewail, A. H. *Science* **1998**, *279*, 847−851.

(34) Møller, K. B.; Zewail, A. H. In *Essays in Contemporary Chemistry*; Quinkert, G., Kisakürek, M. V. Eds.; Verlag Helvetica Chimica Acta: Zürich, Switzerland, 2001; pp 157−188.